Fluid-structure interaction analysis using fixed-grid methods for biomedical applications
流れと柔軟構造物の連成シミュレーション

Lucy Zhang [1] and Shintaro Takeuchi [2]

[1] Department of Mechanical, Aerospace, and Nuclear Engineering, Rensselaer Polytechnic Institute,
JEC 2049, 110 8th St., Troy, NY 12180, USA
[2] Department of Mechanical Engineering, Osaka University,
2-1 Yamada-oka, Suita-city, Osaka 565-0871, JAPAN

1 Introduction

In the past decade, the interest in developing novel simulation techniques for modeling fluid-structure interactions revived due to the increasing demands in capabilities to accurately and efficiently study biomedical applications. Biomedical applications often involve fluid (blood or air) interacting with soft tissues.

Since soft tissues come in with all forms, shapes and sizes, it is more convenient to setup a simulation using a non-boundary-fitted modeling technique. The non-boundary-fitted approaches avoid the re-meshing process by defining independent meshes for the fluid and solid respectively. The solid can freely move on top of the fluid grid without deforming the surrounding fluid. A widely used numerical approach for bio-interface applications is the immersed boundary (IB) method, which was initially proposed by Peskin to study the blood flow around heart valves [1, 2, 3, 4, 5, 6, 7]. The mathematical formulation of the IB method employs a mixture of Eulerian and Lagrangian descriptions for fluid and solid domains. In particular, the entire fluid domain is represented by a uniform background grid, which can be solved by finite difference method with periodic boundary conditions; whereas the submerged structure is represented by a fiber or boundary network. The interaction between the fluid and structure is accomplished by distributing the nodal forces and interpolating the velocities between Eulerian and Lagrangian domains through a smoothed approximation of the Dirac delta function.

The immersed finite element method (IFEM) [8, 9, 10, 11] was developed based on the IB method to represent the background viscous fluid with an unstructured finite element mesh and nonlinear finite elements for the immersed deformable solid. Similar to the immersed boundary method, the fluid domain is defined on a fixed Eulerian grid. However, the solid domain is constructed independently with a Lagrangian mesh, which makes it possible to use a more detailed constitutive model to describe the solid material such as linear elastic, hyperelastic and viscoelastic. This approach is particularly attractive to modeling biomedical applications including stent deployment, blood flow in athersclerosis in arteries, etc. [12, 13, 14, 15, 16, 17, 18, 19, 20]. With finite

element formulations for both fluid and solid domains, the submerged structure is solved more realistically and accurately in comparison to the corresponding fiber network representation in the IB method.

There also exist a number of methods that solve the fluid-solid interaction problem on fixed grid without distribution and interpolation procedures of the nodal forces and velocities (unlike IB methods). Examples include direct-forcing method, originally developed by Mohd-Yusof [21] and improved by Fadlun et al. [22] to allow three-dimensional geometries by enforcing the velocities in the boundary cells to the interpolated values from the ambient velocity field. The method has found many engineering applications [23, 24]. Later, Ikeno and Kajishima [25] proposed a proper discretization scheme of the pressure Poisson equation in a manner that consists with the direct-forcing approach. Sato et al. [26] further evolved the idea of consistency between the discretized (incompressible) flow field and the direct-forcing approach, and presented improved accuracies of the velocity and pressure fields near the object surface.

One of the present authors was also involved in the developments of other fixed-grid approaches; immersed solid approach coupled with a finite element method (IS-FEM) and fully-Eulerian method. The IS-FEM [27] also employs Eulerian and Lagrangian domains for fluid and solid, respectively. In the method, the conservation equations with respect to the mixture velocity field (established through volume-averaging the local fluid velocity and local particle velocity in a cell) are solved with an interaction term at the boundary cells, and the same interaction term (with the opposite sign) is substituted into the finite-element formulation of the solid deformation to update the position and velocities of the object. On the other hand, the fully-Eulerian method [28, 29, 30, 31, 32] describes the solid deformation on Eulerian frame, and couples the motions of the two phases on the Eulerian frame. To account for the presence and the deformation of the object, transport equations of a volume-of-fluid and a left Cauchy-Green deformation tensor are solved. This approach is also attractive to multi-component flow problem involving a variety of solid geometries, such as biomedical applications, as it does not even require the mesh generation for solid object.

The fixed-grid methods are often applied to a flow including an object of complex geometry and moving boundary problem including solid/deformable objects. In this paper, we first provide brief descriptions of the formulations for IFEM, the semi-implicit IFEM, and the modified IFEM, as well as IS-FEM and fully-Eulerian method. Then, we will show several applications of bio-related flow problems by the IFEM algorithms. The choice of the method/algorithm used for each application is dependent on the nature of the fluid-structure interactions (FSI) involved, which comes clear as the readers go through the motivations of each of the algorithm development.

2   Methods

2.1   Immersed finite element method (IFEM)

Let us consider a deformable structure that occupies a finite domain, Ω^s, which is completely immersed in a fluid domain Ω^f. The fluid and the solid together occupy the entire computational domain Ω, and they intersect at a common interface Γ^{FSI}, where "FSI" represents a line if Ω is a two-dimensional domain or a surface if Ω is in three-dimensions. The interface Γ^{FSI} coincides with the solid boundary Γ^s. The nomenclature involved can be partitioned into two categories: one be-

longs to the solid and the other to the fluid. The notations associated with the solid have superscript s to distinguish them from those of the fluid f. The following assumptions are made: (1) The fluid exists everywhere in the domain, Ω. (2) The interface between the fluid and the solid must abide by the matching velocity (or no-slip) and traction boundary conditions. (3) The solid must always remain immersed in the fluid domain to avoid inaccurate interpolations at the fluid-solid interface.

The original derivation of IFEM starts from the principle of virtual of work or the weak form, which is used for standard finite element analysis. The weak forms of the derived equations are equivalent to their strong forms if the weak form solution is smooth enough to satisfy at least C^0 continuity. In the IFEM formulation, the term $f_i^{FSI,f}$ can be interpreted as the external force applied to the fluid that is generated from the artificial fluid. It is important to note that since the solid nodal velocities follow that of the overlapping fluid grid velocities, the compressibility of the solid must follow that of the fluid as well. Therefore, the solid must be incompressible or at least nearly incompressible when the fluid is incompressible.

In the IFEM, small time step has to be used to ensure the stability of the coupling procedure because the solid domain and fluid domain are coupled to each other explicitly at every time step. Since the Navier-Stokes equations are solved implicitly, such small time step requirement due to the coupling stability makes the whole algorithm numerically inefficient especially for the cases when the solid properties are very different from the fluid. Semi-implicit coupling between the fluid and solid domain is then introduced in order to enlarge the stability region.

To alleviate the numerical issues caused by the restrictions in time step size of explicit coupling and the convergence problem due to highly disparate properties between the fluid and the solid domains, a semi-implicit approach is introduced [33]. In the semi-implicit algorithm, the interaction force $\mathbf{f}^{FSI,s}$ is re-defined in the solid domain, which *only* includes the internal forces for the fluid and solid from the original definition. An indicator function, $I(\mathbf{x})$, is to identify the real fluid region Ω^f, the artificial fluid region or the solid region Ω^s, and the fluid-structure interface Γ^{FSI}, in the computational domain Ω. The value of the indicator function is ranged between 0 and 1 where it is 0 if an entire element belongs to the fluid and 1 if an entire element belongs to the solid. Comparing to the original IFEM algorithm, the inertial and the external force terms in the original interaction force formulation are considered in the governing equation and can be evaluated iteratively with the most updated velocity field. This is, therefore, considered as semi-implicit IFEM algorithm.

In the modified IFEM, the algorithm is revamped to capture the solid *dynamics* for high Re flows. For cases where the solid behavior dominates the entire system or high Re flows, using the IFEM algorithm may lead to unrealistic solid deformation and may even cause the severe distortion of the solid mesh, because it is not appropriate to approximate the solid behavior based on the fluid velocity by letting $\mathbf{v}^s = \mathbf{v}^f$. The idea of the modified IFEM is to let the artificial fluid to behave more like the solid, or letting $\mathbf{v}^f = \mathbf{v}^s$. Doing so allows the solid governing equation to be *solved* rather than be *evaluated*. Since the artificial fluid is not real anyway, its role is to produce the same velocity as the solid so that the real fluid realizes the existence of the solid. This modified IFEM algorithm allows the solid behaviors to be estimated more accurately and have stronger influences in the fluid-structure interactions. The detailed rationale and derivations, as well as validation cases were presented in [34].

In order to find the solid displacement field $\mathbf{u}^s$ and the velocity field $\mathbf{v}^s$, the solid equation is solved, $\rho^s u_{i,tt}^s = \sigma_{ij,j}^s$ in Ω^s. The solid stress σ^s is evaluated using the solid strain tensor ε^s,

$\sigma_{kl}^s = c_{ijkl}\varepsilon_{ij}^s + \eta_{ijkl}\varepsilon_{ij,t}^s$, where $\varepsilon_{ij}^s = \frac{1}{2}(u_{i,j}^s + u_{j,i}^s)$. Different combinations of c_{ijkl} and η_{ijkl} provide various choices of solid material constitutive laws such as linear elastic, viscolinear elastic, hyper-elastic, etc. The boundary condition of the solid domain can be applied using either Dirichlet boundary condition or Neumann boundary condition described as: $u_i^s = q_i$ on Γ^{sq}, or $\sigma_{ij}^s n_j = h_i$ on Γ^{sh}, where u_i^s and h_i are, respectively, the diplacement and force at previous time step, such that $q_i = \left[\int_\Omega v_i^f \phi(\mathbf{x} - \mathbf{x}^s) d\Omega\right] \Delta t$ and $h_i = \left[\int_\Omega \sigma_{ij}^f \phi(\mathbf{x} - \mathbf{x}^s) d\Omega\right] n_j$, and n is the outward normal of the fluid-structure interface Γ^{FSI} and Δt is the time step size. These boundary conditions are evaluated based on the fluid velocity (v^f) and stress (σ^f) on the fluid-structure interface solved from the fluid equations at previous time step.

Once the solid solution is obtained, the next step is to make the artificial fluid to follow the solid, i.e. solving the artificial fluid governing equation so that $v^f = v^s$ in $\overline{\Omega}$. To accomplish this, the artificial fluid property, such as the density, should mimic that of the solid.

Using the same semi-implicit interaction force definition and the indicator function as mentioned in the semi-implicit IFEM algorithm, the continuity and momentum equations of the fluid domain, which combines the real fluid domain and artificial fluid domain, can be written as follows,

$$\frac{1}{\kappa^s}\frac{\partial p^f}{\partial t}I(\mathbf{x}) + v_{i,i}^f = 0 \quad \text{in } \Omega.$$

$$\overline{\rho}\frac{\partial v_i^f}{\partial t} + \overline{\rho}v_j^f v_{i,j}^f = \sigma_{ij,j}^f + f_i^{FSI,f} \quad \text{in } \Omega. \tag{1}$$

To enforce the assumption $\mathbf{v}^f = \mathbf{v}^s$ in $\overline{\Omega}$, a correction force is introduced and added into the fluid-structure interaction force. The correction force is effectively the difference between the material derivative of velocity in the solid and the artificial fluid $(\rho^s \left(\frac{D\mathbf{v}^s}{Dt} - \frac{D\mathbf{v}^f}{Dt}\right))$ so that both the inertial and convective acceleration forces are accounted for. It would be zero if the artificial fluid follows the solid exactly. Including this correction force the fluid structure interaction force is re-defined as, $\mathbf{f}^{FSI,s} = \nabla \cdot \boldsymbol{\sigma}^s - \nabla \cdot \boldsymbol{\sigma} + \mathbf{f}^{\Delta v} \quad \text{in } \Omega^s$.

2.2 Immersed-solid (IS) approach coupled with finite element method (FEM)

In IS-FEM method, the whole field is treated as a single continuum and time-updated together with the continuity equation. Because this velocity field does not coincide with the solid velocity at the surface, an interaction term is added to imposed the no-slip condition. Here, the interaction term is modelled to be proportional to the local solid volume fraction and the relative velocity of the local solid to the fluid, and we treat the interaction term to distribute fluid-solid interface region as well as within the solid object, like a body force. The object experiences the same force in the opposite direction. Therefore, the surface integration of hydrodynamic force is replaced with the volume integration of the interaction term over the region enclosing the object. This replacement from surface to volume integration considerably facilitates the computation of the solid motion. More details of the above immersed solid approach are found in the literatures listed in the reference [35, 36]. The method has been applied for studying a clustering process with 1000 spherical particles in a turbulent flow [35, 37, 38]. Also the usefulness of our method has been demonstrated by [39] through the analysis of sedimentation process accommodating a total of 10^5 spherical particles. Solid deformation is solved by finite element method with the above interaction term as the external force term.

The method was applied to a several FSI problems, including elastic particles sedimentation [27] and waving/flowing motion of flexible fibers anchored on a corrugated elastic channel[40, 41].

2.3 Fully-Eulerian method

This simulation method was developed for solving the interaction problem between fluid and elastic object on a fixed Cartesian grid using a finite difference scheme. For describing the multi-component geometry, a volume-of-fluid formulation [42] is applied. Solid deformation is described in the Eulerian frame and the temporal change is updated with a left Cauchy-Green deformation tensor. This deformation tensor is also used to express constitutive equations of nonlinear Mooney-Rivlin materials. The fully-Eulerian method was verified and validated in a number of fundamental interaction problems, and the numerical accuracy involved in the fluid-structure coupling problems has been established [30]. An implicit treatment fully-Eulerian treatment [29] was also developed, and it enables simulation of interaction between hard elastic object and a fluid.

The fully-Eulerian method was further modified to solve the interaction problem between the membrane structure and fluid [43, 44]. For isolating the left Cauchy-Green deformation tensor onto the membrane, a surface left Cauchy-Green deformation tensor is defined by multiplying the surface projection operators on the current and reference configurations. The method was applied to numerical simulation of a blood flow in a capillary vessel, considering the interactions between red blood cells (RBCs)-like elastic membranes (hematocrit of 20%), platelets-like elastic solids and vessel wall deformations.

3 Biomedical Applications of IFEM

In this paper, three biomedical applications are demonstrated. The first example is a blood cell traveling through a bifurcated blood vessel; the second example is to simulate the deployment of an angioplasty stent, which was first presented in [20]; the third example is to study the vocal folds vibration. The first two examples used the original IFEM algorithm where the fluid is blood and the solid is soft tissues. We used the mIFEM algorithm for the third example where the density ratio between the fluid (air) and the soft tissue is large.

3.1 Red blood cell in bifurcated vessel

Understanding the behavior of red blood cell flowing in blood vessels, especially when bifurcation happens, is important in estimating the nonuniform hematocrit distribution that would affect the microvasular oxygen distribution, the effective viscosity of blood in microvessels and the distribution of other metabolites. Using the established IFEM method, one can simulate the motion and the deformation of the red blood cell
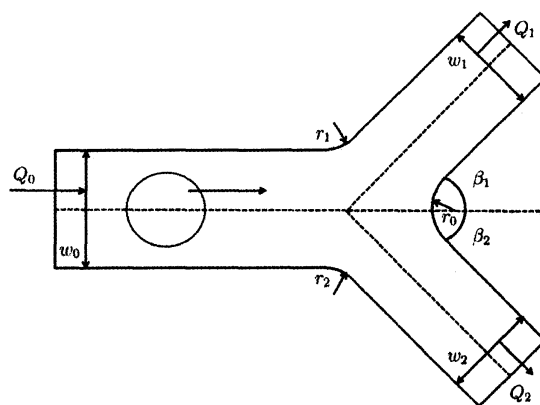
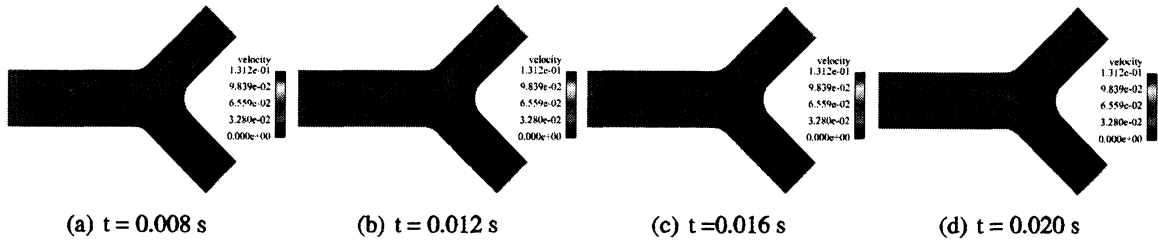

Figure 1: Bifurcation geometry.

(a) t = 0.008 s   (b) t = 0.012 s   (c) t =0.016 s   (d) t = 0.020 s

Figure 2: A RBC flowing in a symmetric bifurcated vessel with $\frac{Q_1}{Q_2} = 3$.

(a) t = 0.00 s   (b) t = 0.01 s   (c) t =0.02 s   (d) t = 0.03 s
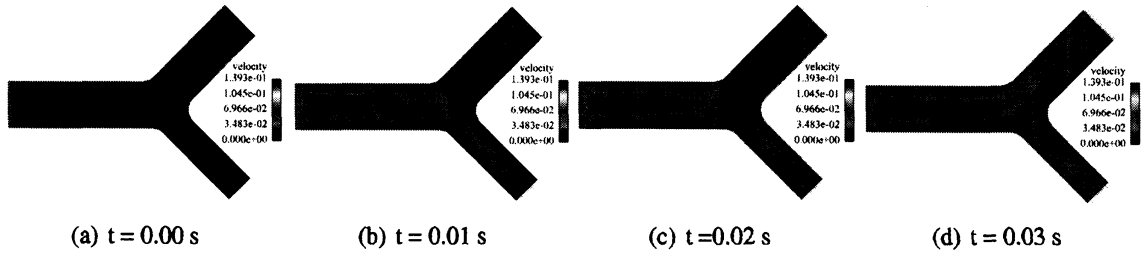
Figure 3: A RBC flowing in an asymmetric bifurcation vessel with $\frac{Q_1}{Q_2} = 1$.

within the vessels, and study in detail how the geometry of bifurcation and fluid field affect and direct which daughter branch the RBC flows.

The geometry of a bifurcated blood vessel is shown in Fig. 1, where w_0 is the diameter of the mother vessel; w_1 and w_2 are the diameters of the daughter vessels on the top and bottom, respectively; β_1 and β_2 are the respective branching angles of the daughter vessels; the branching fillet radii r_0, r_1 and r_2 are given as 3 μm to make the vessel branching transition smooth; Q_0, Q_1 and Q_2 represent the flow rate of each vessel. A RBC is placed near the inlet of the vessel. The radius of the RBC is given as 2.66 μm. The incoming velocity of the mother vessel is set to be a constant as 0.1 cm/s. The branching angles β_1 and β_2 are set to be equal and constant, $\beta_1 = \beta_2 = \pi/4$. In this study, we set the diameter of the mother branch to be $w_0 = 8$ μm, and consider two sets of diameter ratios, $r_d = w_1/w_2$, to be 1 and 1.44. When the diameter ratio is 1, it is considered as symmetric bifurcation; when it is not 1, then it is considered as asymmetric.

Figures 2 and 3 represent the blood cell behaviors when encountering bifurcation in symmetric and asymmetric vessels with different original positions and ratios of flow rate of each daughter vessel. Based on Fig. 2 we can notice that although the daughter branches are symmetric in the geometry, due to the asymmetric boundary conditions where the ratio of the flow rates for the two daughter branches is $\frac{Q_1}{Q_2} = 3$, the blood cell tends to move to the daughter branch with a higher mass flow rate. When the daughter branches are asymmetric in geometry but with the same mass flow rate $\frac{Q_1}{Q_2} = 1$, as shown in Fig. 3, the blood cell moves to the one with a smaller cross section area, which is due to the higher average velocity in that daughter branch.

3.2 Deployment of angioplasty stents

In individuals with an occlusive vascular disease, blood flow to an organ or to a distal body part is impaired by narrowed arteries with fatty deposits or calcium accumulations. Angioplasty and stents

(a) Stent deployment process

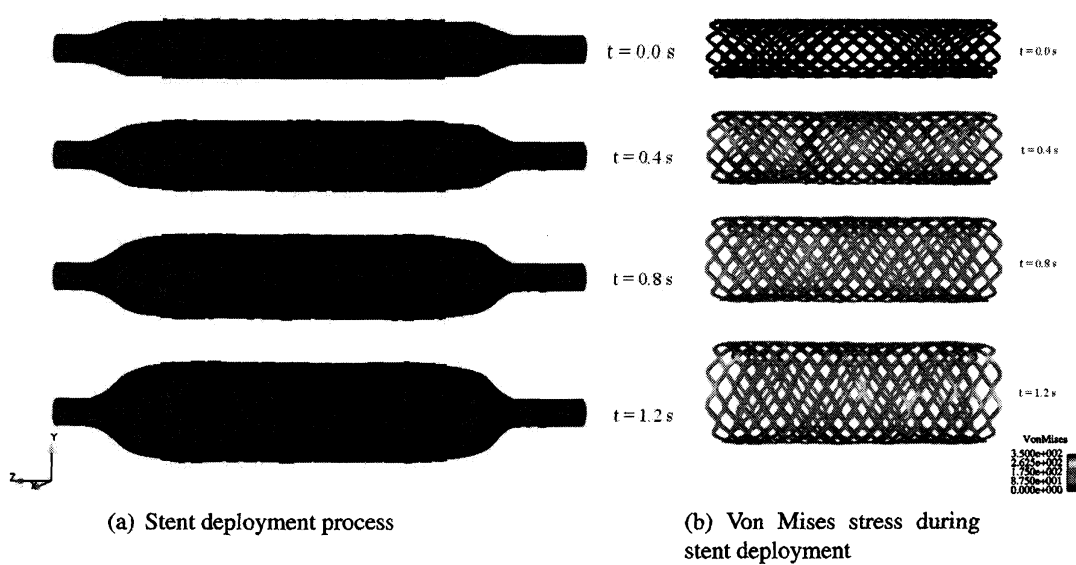(b) Von Mises stress during stent deployment

Figure 4: Stent deployment

physically open the channel of constricted arterial segments. During stenting, a catheter delivers a balloon and a surrounding stent to the location of the blockage area. The balloon deploys the stent, remains inflated for 30 seconds and then is deflated. At the end of the process, the expanded stent is embedded into the wall of the diseased artery and holds it open.

Here, we mainly focus on the deployment process of balloon-expanding stents. In our previous work [16], we built a computer model and simulated a balloon expandable stent interacting with its surrounding fluid using the immersed finite element method. A catheter is located inside the balloon to apply appropriate pressure to inflate the balloon. The balloon has a length of 15 mm, an outer diameter of 1.54 mm, and a thickness of 0.04 mm. Both ends of the balloon are fixed in all directions. The balloons used for stenting are made of very stiff polyamide (nylon) material [45, 46]. The balloon is modeled as hyperelastic material with Mooney-Rivlin description in the simulation. In this particular model, we use the Medtronic AVE Modular stents S7 (Medtronic AVE, Inc., Santa Rosa, CA, USA). Although this stent is no longer been widely used, it is a good representation of a typical geometrical shape of a stent, the model can be simply modified to other expandable devices. The stent, made of wires that form a diamond shape has an outer diameter of 1.64 mm. The stent is made of 16 identical structural members with a total length of 8 mm before its expansion. The cross-section of the wire has a width of 0.08 mm. Finally, the stent is mounted around the balloon. The stent is placed at the center of the balloon. During the entire simulation the inflation pressure is constant and equals to 100 g/cm^2.

Figure 4(a) shows the deployment of the stent during balloon expansion at different time steps. The pressure applied onto the fluid inflates the balloon and the balloon provides a force onto the stent, which enables the stent to expand radially outward until it contacts the inner surface of the artery wall.

The strength and the long term in-vivo performance of the stent can be determined from the stress distributions with the goal of minimizing vascular injury. The stress distribution is uniform

longitudinally along the stent and varies during deployment. These values are critical for recoil and failure analysis.

3.3 Human vocal folds vibration during phonation

Voice is produced by the vibration of vocal folds. The vocal folds are a pair of pliable structures located within the larynx at the top of the trachea. The human vocal folds are roughly $10 \sim 15$ mm in length and $3 \sim 5$ mm thick. The human vocal folds are laminated structures composed of five different layers: the epithelium, the superficial layer (SLP), the intermediate layer (ILP), the deep layer and thyroarytenoid muscle.

The geometry of the self-oscillated vocal folds model is shown in Fig. 5. Since sound is generated by the compression of air, the working fluid is taken as compressible air governed by the ideal gas law at room temperature. The density of the fluid is $\rho^f = 1.3 \times 10^{-3}$ g/cm^3 and the viscosity of the fluid is $\mu = 1.8 \times 10^{-4}$ g/cm $\cdot$ s.

The vocal fold muscle is considered as isotropic viscoelastic material. The vocal fold is assumed to have layered structure, outside cover layer (red) and inside body layer (green). The cover layer is much softer than the body layer. For the cover layer the Young's modulus is $E = 10$ kPa, whereas $E = 40$ kPa for the body layer. The densities of both cover and body layer are assumed to be the same as $\rho^s = 1.0$ g/cm^3. The Poisson ratio is $\nu = 0.3$.

Figure 5: 2-D two-layer self-oscillated vocal folds model.

Two vocal folds have the exact same geometry and material description, sit in the fluid channel symmetric about the central line. A constant total pressure boundary condition of $P_{in} = 1$ kPa is applied at the channel inlet and the outflow boundary is given at the channel exit. No-slip and no-penetration boundary conditions are applied on the channel walls and on the vocal fold surfaces.

A snapshot of the fluid velocity field at two typical instances during a steady vibration cycle are shown in Fig. 6. One can see that the fluid field is not symmetric about the central line during the vibration. The glottal jet tends to attach to one side of the vocal folds randomly, which is the so-called the "Coanda effect" [47, 48].

The asymmetrical airflow causes an asymmetrical pressure distribution in regions near the vocal folds and change in the vibration pattern. The minimum distance between the vocal fold surface and
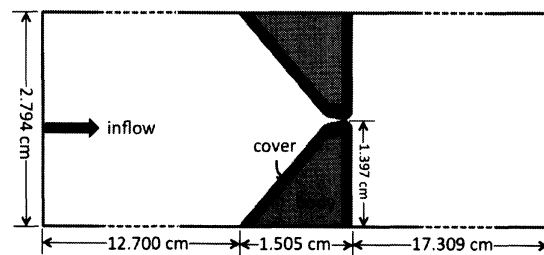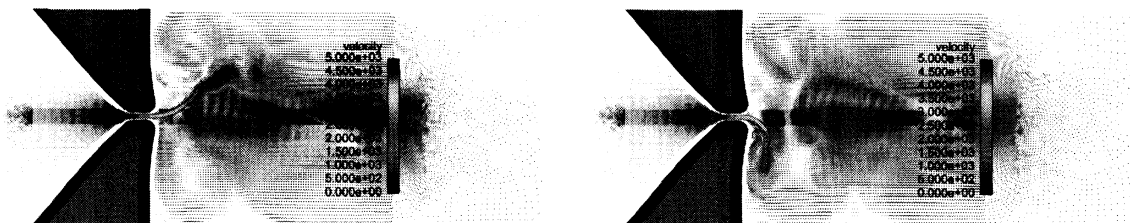

Figure 6: Fluid velocity field at two typical instances during steady vibration.

the central line is measured to represent the half glottis width (Gw), shown in Fig. 7, where Gw_{up} and Gw_{down} represent the opening width for the up and down vocal folds, respectively. This figure shows that the simulation captures the vocal folds to have a repeated opening and closing process. When the glottis width is zero or near-zero, then the vocal folds are closed, there is no air flowing through. The pressure starts to build up in the upstream of the vocal channel. As the pressure increases, it starts to push the vocal folds to open and eventually reaches a maximum glottis width, the high pressure is released. The vocal folds then return back to its closed position, and the whole process restarts.

4 Summary

In this paper, we briefly reviewed some fluid-structure interaction (FSI) methods and algorithms that had been developed over the past decade. The IFEM method is a numerical scheme that adopts the non-boundary-fitted mesh approach and fully couple the fluid-structure interaction by interpolation the interacting domains. The fluid and solid domains are solved independently using finite element method and coupled with each other within one time step through fluid-structure interaction force. Three biomedical applications are illustrated in the paper. We show that the IFEM can model some complicated biomedical applications that involve fluid-structure interactions.
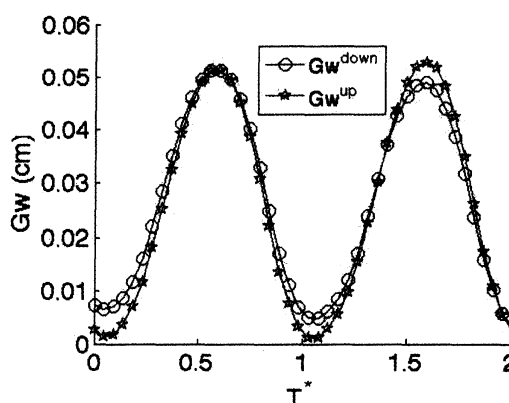

Figure 7: Half glottis width of top and bottom vocal folds.

REFERENCES

[1] Peskin, C.S., Numerical analysis of blood flow in the heart, *Journal of Computational Physics* 25 (1977) 220-252

[2] McCracken, M.F. and Peskin, C.S., A vortex method for blood flow through heart valves, *Journal of Computational Physics* 35 (1980) 183-205

[3] McQueen, D.M. and Peskin, C.S., Computer-assisted design of pivoting-disc prosthetic mitral valves, *Journal of Computational Physics* 86 (1983) 126-135

[4] Peskin, C.S. and McQueen, D.M., A three-dimensional computational method for blood flow in the heart. I. Immersed elastic fibers in a viscous incompressible fluid, *Journal of Computational Physics* 81-2 (1989) 372-405

[5] Peskin, C.S. and McQueen, D.M., Cardiac fluid dynamics. Critical Reviews in Biomedical Engineering, *SIAM Journal on Scientific and Statistical Computing* 20-6 (1992) 451-459

[6] Peskin, C.S. and McQueen, D.M., Mechanical equilibrium determines the fractal fiber architecture of aortic heart valve leaflets, *American Journal of Physiology* 266-1 (1994) H319-H328

[7] Peskin, C.S. and McQueen, D.M., Case Studies in Mathematical Modeling-Ecology, Physiology, and Cell Biology, Prentice-Hall (1996)

[8] Zhang, L.T., Gerstenberger, A., Wang, X. and Liu, W.K., Immersed finite element method, *Computer Methods in Applied Mechanics and Engineering* **193** (2004) 2051-2067

[9] Zhang, L.T. and Gay, M., Immersed finite element method for fluid-structure interactions, *Journal of Fluids and Structures* **23** (2007) 839-857

[10] Zhang, L.T. and Gay, M., Imposing rigidity constraints on immersed objects in unsteady fluid flows, *Computational Mechanics* **42** (2008) 357-370

[11] Wang, X. and Zhang, L.T., Numerical method for fluid-structure interactions with sharp interfaces: formulation and convergence tests, *Computational Mechanics* **45** (2010) 321-334

[12] Liu, W.K., Liu, Y., Farrell, D., Zhang, L.T., Wang, S., Fukui, Y., Patankar, N., Zhang, Y., Bajaj, C., Lee, J., Hong, J., Chen, X. and Hsu, H., Immersed finite element method and its applications to biological systems, *Computer Methods in Applied Mechanics and Engineering* **195** (2006) 1722-1749

[13] Liu, W.K., Liu, Y., Zhang, L.T., Wang, X., Gerstenberger, A. and Farrell, D., Immersed finite element method and applications to biological systems. Finite Element Methods: 1970's and Beyond, International Center for Numerical Methods and Engineering, (2004)

[14] Liu, Y. and Liu, W.K., Rheology of red blood cell aggregation in capillary by computer simulation, *Journal of Computational Physics* **220** (2006) 139-154

[15] Liu, Y., Zhang, L.T., Wang, X. and Liu, W.K., Coupling of Navier-Stokes equations with protein molecular dynamics and its application to hemodynamics, *International Journal for Numerical Methods in Fluids* **46**-12 (2004) 1237-1252

[16] Gay, M., Zhang, L.T. and Liu, W.K., Stent modeling using immersed finite element method, *Computer Methods in Applied Mechanics and Engineering* **195** (2006) 4358-4370

[17] Zhang, L.T., Shear stress and shear-induced particle residence in stenosed blood vessels, *International Journal of Multiscale Computational Engineering* **6** (2008) 141-152

[18] Zhang, L.T. and Gay, M., Characterizing left atrial appendage functions in sinus rhythm and atrial fibrillation using computational models, *Journal of Biomechanics* **41** (2008) 2515-2523

[19] Gay, M. and Zhang, L.T., Numerical studies of healthy, stenosed, and stented coronary arteries, *International Journal of Numerical Methods in Fluids* **61** (2009) 453-472

[20] Gay, M. and Zhang, L.T., Numerical studies on fluid-structure interactions of stent deployment and stented arteries, *Engineering with Computers* **25** (2009) 61-72

[21] Mohd-Yusof, J., Combined immersed-boundary / B-spline methods for simulations of flow in complex geometries, *Center for Turbulence Research Annual Research Briefs* (1997) 317-327, Stanford University

[22] Fadlun, E. A., Verzicco, R., Orlandi, P. and Mohd-Yusof, J., Combined immersed-boundary finite-difference methods for three-dimensional complex flow simulations, *Journal of Computational Physics* **161** (2000) 35-60

[23] Verzicco, R., Iaccarino, G., Fatica, M. and Orlandi, P., Flow in an impeller stirred tank using an immersed boundary method, *Center for Turbulence Research Annual Research Briefs* (2000) 251-261, Stanford University

[24] Verzicco, R., Fatica, M., Iaccarino, G. and Moin, P., Large eddy simulation of a road vehicle with drag-reduction devices, *AIAA Journal* **40** No. 12 (2002) 2447-2455

[25] Ikeno, T. and Kajishima, T., Finite-difference immersed boundary method consistent with wall conditions for incompressible turbulent flow simulations, *Journal of Computational Physics* **226** (2007) 1485-1508

[26] Sato, N., Kajishima, T., Takeuchi, S., Inagaki, M. and Horinouchi, N., A Direct Discretization Approach near Wall Boundaries for a Cartesian Grid Method (Consideration of Consistency between Velocity and Pressure Fields) *Trans. JSME Ser.B* **79**-800 (2013) 605-621

[27] Takeuchi, S., Yuki, Y., Ueyama, A. and Kajishima, T., 2010, A conservative momentum exchange algorithm for interaction problem between fluid and deformable particles, *International Journal for Numerical Methods in Fluids* **64** 1084-1101

[28] Sugiyama, K., Nagano, N., Takeuchi, S., Ii, S., Takagi, S. and Matsumoto, Y., Particle-in-cell method for fluid-structure interaction simulations of neo-Hookean tube flows, *Theoretical and Applied Mechanics Japan* **59** (2011) 245-256

[29] Ii, S., Sugiyama, K., Takeuchi, S., Takagi, S. and Matsumoto, Y., An implicit full Eulerian method for the fluid-structure interaction problem, *International Journal for Numerical Methods in Fluids* **65** (2011) 150-165

[30] Sugiyama, K., Ii, S., Takeuchi, S., Takagi, S. and Matsumoto, Y., A full Eulerian finite difference approach for solving fluid-structure coupling problems, *Journal of Computational Physics* **230** (2011) 596-627

[31] Nagano, N., Sugiyama, K., Takeuchi, S., Ii, S., Takagi, S. and Matsumoto, Y., Full-Eulerian finite-difference simulation of fluid flow in hyperelastic wavy channel, *Journal of Fluid Science and Technology* **5** (2010) 475-490

[32] Sugiyama, K., Ii, S., Takeuchi, S., Takagi, S. and Matsumoto, Y., Full Eulerian simulations of biconcave neo-Hookean particles in a Poiseuille flow, *Computational Mechanics* **46**-1 (2010) 147-157

[33] Wang, X., Wang, C. and Zhang, L.T., Semi-implicit formulation of the Immersed Finite Element Method, *Computational Mechanics* **49** (2011) 421-430

[34] Wang, X. and Zhang, L.T., Modified Immersed Finite Element Method for solid-dominated fully-coupled fluid-structure interactions, *Computer Methods in Computer Methods in Applied Mechanics and Engineering* **267** (2013) 150-169

[35] Kajishima, T., Takiguchi, S., Hamasaki, H. and Miyake, Y., 2001, "Turbulence structure of particle-laden flow in a vertical plane channel due to vortex shedding", *JSME International Journal Series B*, **44**-4 526-535

[36] Yuki, Y., Takeuchi, S. and Kajishima, T., 2007, "Efficient immersed boundary method for strong interaction problem of arbitrary shape object with the self-induced flow", *Journal of Fluid Science and Technology*, **2**-1 1-11

[37] Kajishima, T. and Takiguchi, S., 2002, "Interaction between particle clusters and fluid turbulence", *International Journal of Heat and Fluid Flow*, **23**-5 639-646

[38] Kajishima, T., 2004, "Influence of particle rotation on the interaction between particle clusters and particle-induced turbulence", *International Journal of Heat and Fluid Flow*, **25**-5 721-728

[39] Nishiura, D., Shimosaka, A., Shirakawa, Y. and Hidaka, J., Hybrid simulation of hindered settling behavior of particles using discrete element method and direct numerical simulation (in Japanese), *Kagaku Kogaku Ronbunshu*, **32**-4 (2006) 331-340

[40] Ito, A., Takeuchi, S. and Kajishima, T., Numerical analysis of the effect of flexible wall elements on flow behavior, Proc. 6th European Congress on Computational Methods in Applied Sciences and Engineering (ECCOMAS 2012), Publication No. 3800, Vienna, Austria, 10-14 September, 2012.

[41] Ito, A., Miyauchi, S., Takeuchi, S. and Kajishima, T., Numerical analysis of the interaction between fluid and flexible fibres clamped on elastic walls, Proc. 2nd International Conference on Mechanical Engineering Research (ICMER 2013), Pahang, Malaysia, 1-3 July, 2013

[42] Hirt, C.W. and Nichols, B.D., Volume of fluid (VOF) Method for the dynamics of free boundaries, *Journal fo Computational Physics* **39** (1981) 201-225

[43] Ii, S., Gong, X., Sugiyama, K., Wu, J., Huang, H. and Takagi, S., A full Eulerian fluid-membrane coupling method with a smoothed volume-of-fluid approach, Communications in Computational Physics **12**-2 (2012) 544-576

[44] Ii, S., Sugiyama, K., Takagi, S., and Matsumoto, Y., A computational blood flow analysis in a capillary vessel including multiple red blood cells and platelets, *Journal of Biomechanical Science and Engineering* **7**-1 (2012) 72-83

[45] Serruys, P.W. and Rensing, B.J., *Handbook of coronary stents*, Martin Dunitz, London, 4th edition (2002)

[46] Saab, M.A., Applications of high-pressure balloons in the medical device industry, Advanced Polymers, Inc., Salem, NH, USA, (1999),

[47] Tao, C., Zhang, Y., Hottinger, D.G. and Jiang, J.J., Asymmetric airflow and vibration induced by the Coanda effect in a symmetric model of the vocal folds, *Journal of the Acoustical Society of America* **122** (2007) 2270-2278

[48] Drechsel, J.S. and Thomson, S.L., Influence of supraglottal structures on the glottal jet exiting a two-layer syngthetic, self-oscillating vocal fold model, *Journal of the Acoustical Society of America* **123** (2008) 4434-4445